Hindawi Publishing Corporation
EURASIP Journal on Wireless Communications and Networking
Volume 2010, Article ID 728468, 11 pages
doi:10.1155/2010/728468

Research Article

Design of an Omnidirectional Multibeam Transmitter for High-Speed Indoor Wireless Communications

Jaw-Luen Tang and Yao-Wen Chang

Department of Physics, National Chung Cheng University, Chiayi County 62102, Taiwan

Correspondence should be addressed to Jaw-Luen Tang, phyjlt@ccu.edu.tw

Received 30 October 2009; Revised 17 April 2010; Accepted 9 May 2010

Academic Editor: Anthony C. Boucouvalas

For future high speed indoor wireless communication, diffuse wireless optical communications offer more robust optical links against shadowing than line-of-sight links. However, their performance may be degraded by multipath dispersion arising from surface reflections. We have developed a multipath diffusive propagation model capable of providing channel impulse responses data. It is aimed to design and simulate any multibeam transmitter under a variety of indoor environments. In this paper, a multi-beam transmitter system associated with hemisphere structure is proposed to fight against the diverse effects of multipath distortion albeit, at the cost of increased laser power and cost. Simulation results of multiple impulse responses showed that this type of multi-beam transmitter can significantly improve the performance of BER suitable for high bit rate application. We present the performance and simulation results for both line-of-sight and diffuse link configurations. We propose a design of power radiation pattern for a transmitter in achieving uniform and full coverage of power distributions for diffuse indoor optical wireless systems.

1. Introduction

In recent years, the development of indoor optical wireless communication system has received great attention due to its capability for future high speed and flexible optical communications at low cost [1–11]. Wireless optical link can also offer a secure and a promising alternative to radio communications for wireless indoor applications. Indoor optical wireless network (such as Infrared links) can be classified as several configurations for link design.

In simple infrared links the classification is normally based on the directionality and line-of-sight (LOS) between the receiver and transmitter [7, 8]. In LOS link system, optical carrier from the transmitter reaches the receiver directly, while in non-LOS link system, an optical carrier reaches the receiver after some diffusive reflections by the ceiling and/or walls in the room. Directed LOS links are the most widely used IR links and offer low path loss, but require precise alignment of the transmitter/receiver and are susceptible to blockage of the beams. Nondirected non-LOS links, also known as diffuse links, where the optical carrier is reflected diffusively to omnidirection and fills the whole room can avoid the need for aiming the transmitter and provide robustness against shadowing due to the blockage, but suffer from increased path loss and data-rate limitation caused by multipath reflections. Hybrid systems, where the transmitter and receiver have different degrees of directionality, are commonly used to improve the link performance. Diffusive systems, such as diffuse indoor IR wireless system, are referred to those systems using a combination of nondirected and non-LOS transceiver configurations.

One of the key issues in nondirected diffuse optical wireless communications is to design an omnidirectional highspeed multibeam transmitter that can overcome the shortcomings occurred in indoor wireless local-area network (WLAN), such as ambient radiation interference, detector noises, wall reflections, and multipath dispersion [2, 3, 10–17]. In addition, substantial nonuniform power distribution at various points in a room is also a problem for the diffuse indoor IR wireless system. There have been a number of studies [18–33] explored to solve this power nonuniformity problem, in which most of them suggested the use of multiple transmitter associated with multispot diffusing imaging or nonimaging receivers. For example,

Carruthers and Kahn [20] have proposed angle diversity technology by using multiple narrow beam transmitter and multiple nonimaging receivers. The advantages of these types of systems are high ambient light rejection and reduced multipath distortion due to the use of narrow FOV detector in the receivers. Later, Kahn et al. [21] reported the use of imaging diversity receiver to reduce ambient light and path loss. Djahani and Kahn [13, 22] have used multibeam (quasidiffusive) transmitters and imaging diversity receivers to improve the link performance for both LOS and non-LOS IR links. The link performance is quantified as the transmitted power required for achieving a bit error rate (BER) not exceeding 10^{-9} with 95% probability. The system can reduce the required transmitted power by up to 13 dB in LOS links and more than 20 dB in non-LOS links. Al-Ghamdi and Elmirghani [27–30] have analyzed the performance of IR links by using a line strip multibeam transmitter combined with angle diversity receiver. With this system, they demonstrated that high performance can be achieved due to the significant reduction in background noise and inter symbol interference (ISI) effects as well. Other systems also show some promising results by either increasing signal-to-noise ratio or reducing path loss/multipath dispersion such as holographic diffusers [18], multispot diffusing using holographic diffusing spot array generator [22–24], multiple transmitters [19], and multiple optical sources [24].

Most of the above approaches exploited so far to some degree are quite complicated and require sophisticated transceiver system and demodulation scheme. Out of them, the one utilizing multiple or multibeam transmitters is relatively simple and quite appealing as it can produce near-uniform power distribution and mitigate the shadowing effects. Additionally, it can overcome the drawbacks and combines the advantages of both LOS links and diffuse links. The power levels of the transmitters can be carefully adjusted to meet the eye safety standards. Bakalidis et al. [19] and Yang and Lu [26] have shown that near uniform optical power distribution (within the working range of the receivers) is possible when a number of transmitters were placed in a predefined square grid (or pixel) near the ceiling of the room, assuming the delay dispersion of such a source configuration is negligible. The ratio of the maximum to minimum received power is termed as degree of uniformity and is used as a measure of the amount of power variations on the floor. In our work, we propose a multibeam transmitter mounted on the ceiling and a single-element receiver located on the floor pointing toward the ceiling. In this configuration, the optical signal communication between the transmitter and receiver can occur only through the reflected rays from the ceiling/walls. The system has the potential of providing a field of view (FOV) of near semisphere or 180 degree with sufficient power level.

To combat the adverse effects of multipath dispersion for high bit rate system, accurate propagation models are essential and needed. The power distribution in a room can be simulated accurately using the impulse response of the channel. The channel impulse response is used to analyze and compensate for the effects of multipath temporal dispersion [9]. There have been some algorithms developed for this purpose, such as the recursive method [9], statistical approach [34], DUSTIN algorithm [35], Monte Carlo calculation [36], Modied Monte Carlo Scheme [37], Ceiling bounce model [38] and Iterative Site-Based Modeling [39], and Modified recursive method [31, 32]. The recursive method by Barry et al. [9] is most commonly used for the single transmitter environment and it agrees well with experimental results. We extended this recursive method to evaluate the impulse response suitable for the multibeam (multielement) transmitter environment and in some way it is similar to the modified recursive method developed by Sivabalan and John [31, 32].

In this paper, we present a multipath diffusive propagation model [40], which is aimed to design and simulate infrared wireless transceiver under a variety of indoor environments. Based on ray tracing algorithms this computer code calculates the impulse responses of an arbitrary room filled with Lambertian optical sources and reflectors. The method described here in principle can calculate the impulse response accounting for any number of reflections from any number of optical sources assembled by a single multibeam transmitter configuration. This allows a fairly accurate analysis of power distributions and impulse responses. The method can further be easily modified to incorporate the effects of angle diversity reception with an imaging receiver, but at the cost of several tens times of computing time. We have investigated the spatial and temporal power distributions of several possible multibeam transmitter configurations in a room with multiple reflectors such as wall, ceiling, and floor. Simulation results for both LOS and diffuse link configurations are presented. The results can be applied to design and select the optical transmitter that overcomes the drawbacks encountered in those links and provides the full coverage of field of view as well as the power receiving performance.

A prototype multibeam transmitter suitable for producing uniform, near hemisphere or 180 degree, high speed, and long distance infrared radiation is proposed, and the simulation results is shown. The method presented here can also be applied for the design and simulation of fiber launch system to achieve high bit rate and low noise performance in fiber optical communications.

2. Channel Modeling and Simulation Algorithms

Shown in Figure 1 is the system model of nondirected diffuse optical wireless channel system with the proposed multibeam transmitter in an indoor environment. The transmitter is located on the ceiling, while the receiver is on the floor of the same room. The simulation scenery of diffusive optical channel presented in this paper is in an empty rectangular room, although our techniques can be extended to other shape of rooms. Note that the simulation model and technique reported here can also be applied for any transmitter system in optical fiber communications. The wireless channel model, as described below, includes optical source, surface reflector, and photodiode receiver.

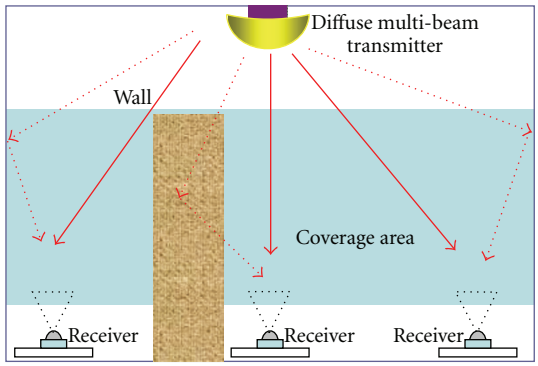

Figure 1: System model of nondirected diffuse optical channel with a multibeam transmitter.

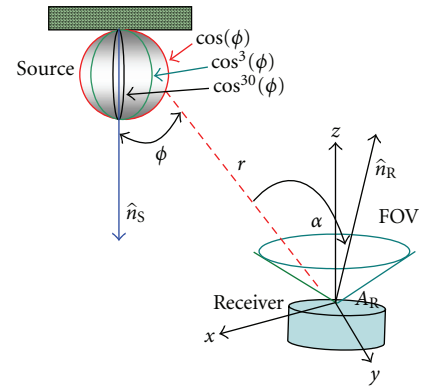

Figure 2: Geometry of optical source model with Lambertian radiation pattern and receiver model.

2.1. Optical Source and Surface Reflector Models. An optical source or a multibeam transmitter is modeled by a position vector r_s, an orientation unit vector $\hat{n}_s$, a total average power P_s and a radiation intensity pattern $P(\phi)$. The radiation intensity pattern is defined as the optical power per unit solid angle emitting from the source at position r_s with an angle ϕ with respective to its surface normal vector $\hat{n}_s$. We model the source using a generalized Lambertian radiation pattern of order N with uniaxial symmetry [3]:

$$P(\phi) = P_s \frac{(N+1)}{2\pi} \cos^N(\phi) \operatorname{rect}\left(\phi, \frac{\pi}{2}\right), \quad \phi \in \left[-\frac{\pi}{2}, \frac{\pi}{2}\right], \tag{1}$$

where P_s is the total emitting power or irradiance of the source, and ϕ is the emitting angle or the angle with respect to source surface normal. The order N or mode number of the radiation lobe specifies the directionality of the source and is related to half-power sermiangle $\Phi_{1/2}$ of the source by $N = \ln 2/[\ln(\cos \Phi_{1/2})]$. A traditional Lambertian source has a mode of $N = 1$. In particle, such beam can be generated using optical diffusers or computer-generated interference hologram.

To simplify the simulation, we assume all reflectors are purely ideal diffusive Lambertian source with $N = 1$, although true reflections in general include both specular and diffusive [41]. Several experimental measurements have verified that many typical materials such as plaster walls, carpets, and unvarnished woods can be approximated as Lambertian reflectors very well [42, 43]. The radiation intensity pattern $P(\phi)$ emitted by a differential element of an ideal diffusive reflector is independent of the incident angle of the light source. The power received by a sufficiently small receiver or reflector with a detecting area dA, can be shown to be

$$dP = \frac{1}{r^2} P \frac{(N+1)}{2\pi} \cos^N(\phi) \cos(\alpha) \operatorname{rect}\left(\phi, \frac{\pi}{2}\right) dA, \tag{2}$$

where ϕ and α are the emitting and incident angles, respectively, and r is the distance between transmitter and receiver, as illustrated in Figure 2. The surface reflector then becomes a secondary source and re-emits power into space. The power radiated by the reflecting surface dA depends on its reflection coefficient ρ and is assumed to be independent of the incident angle α. The radiation pattern from the reflecting surface again is a Lambertian with mode number $N = 1$ and a differential power distribution of $\rho\, dP$ into the free space.

2.2. Receiver Model. The receiver model consists of an optical lens system or concentrator, a photodetector, and a signal processing unit. The optical system to collect the radiation from the source is assumed to be ideal. The receiver mode is specified by a position vector r_R, an orientation unit vector $\hat{n}_R$, a receiving effective area A, and field of view, defined as a scalar angle such that a receiver only detect light radiation whose angle of incidence is inside the FOV. This model calculates current signal and noise received by the detector. The photon current signal at the detector includes the optical signal input, background and dark current. In general, the photon current can be written as the sum of input signal $R_s s(t)$ and noise $n(t)$:

$$I(t) = R_s s(t) + n(t), \tag{3}$$

where R_s is detector responsivity. The background noise $n(t)$ is modeled as white and Gaussian noise, and independent of the input signal. The averaged current signal $s(t)$, a convolution integral of received power $x(t)$ and system impulse response function $h(t)$, measured by the detector is given by

$$s(t) = \int_{-\infty}^{\infty} x(\tau) h(t-\tau) d\tau. \tag{4}$$

The received power at the detector contains a transmitted power P_s from the optical signal and a background radiation P_{bg} received at the detector. The noise is determined by the variance in current noise at the detector for receiving any optical signal. The photon-generated noise or shot-noise variance in the detector that results from the received signal is

$$\sigma_{\text{ss}}^2 = 2qR_s P_s \Delta f, \tag{5}$$

where q is the electron charge and Δf is the electron bandwidth. The following parameters are used: $R_s = 0.5$ A/W and $\Delta f = 100$ MHz. The variance in current at the detector that arises from background radiation P_{bg} is given by

$$\sigma_{\text{bg}}^2 = 2qR_sP_{\text{bg}}\Delta f. \tag{6}$$

The current variance in the detector that arises from the dark current of the photodiode can be expressed by

$$\sigma_{\text{dc}}^2 = 2qR_sI_{\text{dc}}\Delta f, \tag{7}$$

where I_{dc} is the dark current ($\sim$1 nA) in the detector. In addition, the current variance in the detector that results from Johnson (thermal) noise is given by

$$\sigma_{\text{js}}^2 = \frac{4kT\Delta f}{R_L}, \tag{8}$$

where F is the noise figure of the system, and T is the equivalent temperature, and R_L is the load resistance. The Johnson noise is modeled with the following parameters: T = 300 K and R_L = 10 kΩ. From (5)–(8), the total variance in current noise in the detector is given by

$$\sigma_{\text{tot}}^2 = \sigma_{\text{ss}}^2 + \sigma_{\text{bg}}^2 + \sigma_{\text{dc}}^2 + \sigma_{\text{js}}^2. \tag{9}$$

When the shot noise is the dominant noise source, the total noise variance can be approximated as $\sigma_{\text{tot}}^2 \approx \sigma_{\text{ss}}^2$.

2.3. LOS and Diffusive Impulse Response. Assuming that the distance $r(x, y, z)$ between the transmitter and receiver is much greater than the effective receiving area of the detector, the received power at the detector is approximately a constant over the surface of the receiver. The LOS impulse response in an environment with no reflectors can be evaluated as

$$h(r,t) = \frac{1}{r^2}P\frac{(N+1)}{2\pi}\cos^N(\phi)\cos(\alpha)\text{rect}\left(\phi, \frac{\pi}{2}\right) \times dA\,\delta\left(t - \frac{r}{c}\right). \tag{10}$$

Taking the diffuse reflection into account, the impulse response of the optical channel is comprised of an LOS component and a diffusive (non-LOS) component, $h_{\text{tot}}(t) = h_{\text{LOS}}(t) + h_{\text{diff}}(t - \Delta T)$. The surface power-delay illumination pattern can be obtained by dividing walls and other reflecting surfaces into pixels and then rays are traced across surfaces between pixels. The initial surface illumination pattern at Cartesian coordinates, due to the optical source, is calculated by

$$I^{(1)}(t,x,y,z) = h_{\text{tot}}(t,x,y,z). \tag{11}$$

The overall impulse responses, a summation of primary source and subsequent illumination due to secondary sources, can be calculated as

$$I^{(k)}(t,x,y,z) = \sum_{n=i}^{n} h_{\text{tot}}\left(t; I^{(k-1)}\right); \quad k > 1. \tag{12}$$

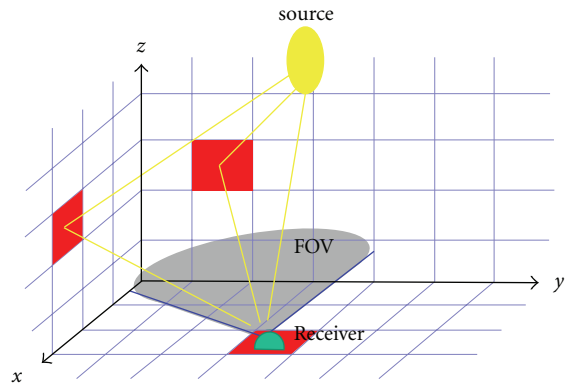

Figure 3: A diffusive optical link with the geometry of source and receiver and ray tracing between reflector and receiver pixels.

where $I^{(k-1)}$ is the response from $(k-1)$ reflections and n is the total number of pixel elements. For a multibeam transmitter equipped with m sources the channel response function can be computed as follows [31, 32]:

$$h(t) = \sum_{l=1}^{m}\sum_{n=1}^{\infty} I_{(l)}^{(k)}(t,x,y,z). \tag{13}$$

The tracing of optical rays is up to 5 reflections for time duration of 200 ns to sufficiently simulate the multipath propagation. After the surface illumination pattern is evaluated, the impulse response of a particular receiver can be determined by ray tracing elements from the receiver to the respective reflectors.

Given the distribution of transmitted optical power we can thus estimate the received optical power from (13). For transmitted power P_{tx} with a unit Dirac delta function, the average received power P_{rx} is $P_{\text{rx}} = P_{\text{tx}}H(0)$, where $H(0) = \int_{-\infty}^{\infty} h(t)dt$.

2.4. Signal-to-Noise Ratio (SNR) and Bit Error Rates (BER). We assume here that the receiver transmits at bit rate using on-off keying (OOK). Among all modulation techniques for wireless infrared links, OOK is the simplest to implement. In a single receiver, the average signal-to-noise ratio (SNR) is defined as the ratio of the reviced signal to the avgerated noise and is expressed as

$$\text{SNR} = \frac{(R_sP_s)^2}{\sigma_{\text{tot}}^2}. \tag{14}$$

It can be seen that when the shot-noise in (6) is the dominant noise source, then the SNR is proportional to the square of the detector area. This is because the numerator is always proportional to the square of the detector area and the shot noise variance is always proportional to the detector area. Hence, if shot noise is dominant, then the SNR is proportional to the detector area. Assuming OOK with equiprobable zeros and ones, the BER is evaluated as

$$\text{BER} = Q\left(\sqrt{\text{SNR}}\right), \tag{15}$$

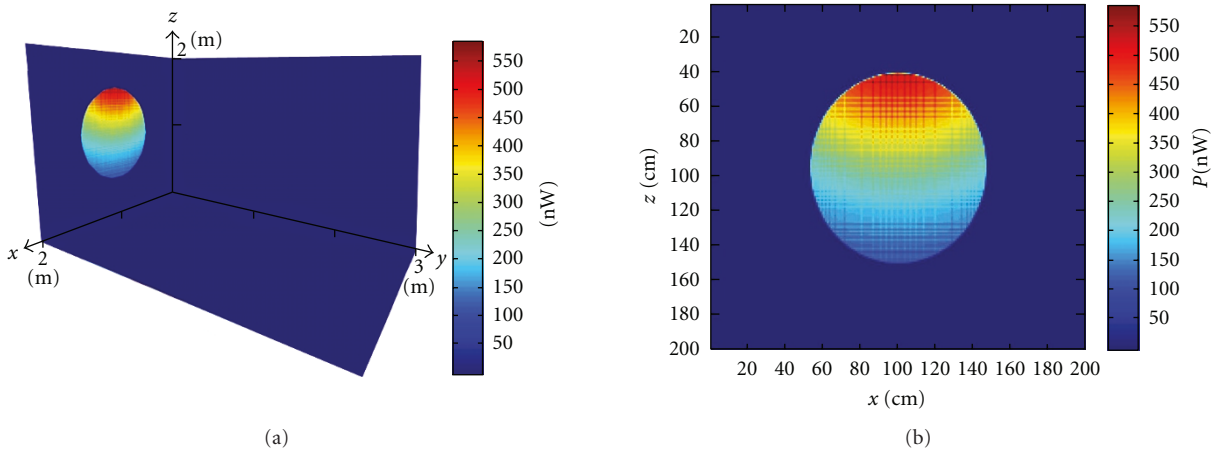

(a) (b)

Figure 4: The surface power distributions with rays tracing for one reflection for (a) three walls and (b) one wall.

where

$$Q(x) = (2\pi)^{-1/2} \int_x^\infty \exp(-y^2/2)\,dy. \tag{16}$$

For example, an SNR of 36 (15.6 dB) is required to achieve a BER of 10^{-9}.

2.5. Channel Bandwidth. The bandwidth of the indoor channel is computed from the Fourier transform of the channel impulse responses as

$$H(\omega) = \int_{-\infty}^{\infty} h(t)e^{i\omega t}dt \approx \sum_{-\infty}^{\infty} h(n\Delta t)e^{i\omega\Delta t}\Delta t,$$
$$H(\omega) = \Delta t H(\exp(i\omega\Delta t)), \tag{17}$$

where $H(\exp(i\omega\Delta t))$ is the discrete-time Fourier transform of the discrete time signal $h(n\Delta t)$. These results are used to plot the normalized amplitude $|\Delta t H(e^{i\omega\Delta t})|$ versus frequency f and from which the 3 dB channel bandwidth is obtained.

3. Results and Discussion

3.1. Surface Illumination of a Single-Beam Transmitter. A computer program was written using MATLAB software package that implements the algorithms presented in the previous section. Simulations were performed using ray tracing approach for a typical diffusive optical channel, as illustrated in Figure 3, where a diffusive optical source with a divergent angle of 30 degrees is used to emit light radiation into a rectangular empty room. We assign the direction of north with x axis and the direction of west with y axis. The elevation angles are measured with respective to the horizontal plane, such that a source pointing straight down has an elevation angle of 90 degrees, and a receiver pointing straight up has an elevation of −90 degrees. The azimuth angle at position r is defined as the angle between x axis and the projection of r vector onto the x-y plane. The choice of time interval Δt or the bin width of the power histogram that approximates the impulse response will determine the computing time of simulation. The time interval of 2 ns is used in this case.

The walls and other reflecting surfaces of the room are segmented into square pixel size of 1 cm^2 and rays are traced across surfaces between pixels to calculate the surface power-delay illumination pattern. The optical source or transmitter is positioned on the ceiling (x = 1 m, y = 1.5 m, z = 2 m), emitting with an elevation angle of θ = 30 degrees and an azimuth angle of ϕ = 0 degrees. The transmitter in our simulation setup was a highspeed 850 nm light emitting diode (LED) with a spectral bandwidth of 50 nm, which emitted an optical beam with an approximately Lambertian radiation pattern. The typical response time for the transmitter was 5 ns. A wide angle receiver (180 degrees FOV) consisted of a silicon photodiode with 1 cm^2 collection area is located on the floor (x = 1.0 m, y = 0 m, z = 0 m). The typical rise/fall time for the receiver was 10 ns. The reflection coefficients for walls, ceiling and floor are 0.8. The order of Lambertian used in this simulation is N = 1. Two configurations were considered in this simulation (i) a small room with dimensions of $2.0 \times 3.0 \times 2.0$ (m), and (ii) a larger room with dimensions of $10.0 \times 5.0 \times 2.0$ (m). Table 1 lists the room dimensions and simulated parameters.

Shown in Figure 4 are the surface power distributions of three walls for the small room simulated with ray tracing to only one reflection from the pixel element, while for that of Figure 5 the number of reflections is up to 5. The surface power distribution shown in Figure 5 is calculated as

$$P(x, y, z) = \sum_t \sum_{k=1}^{5} I^{(k)}(x, y, z; t). \tag{18}$$

Figure 6(a) shows the surface power distributions of three walls for the larger room when an LOS optical line was used. For a nondirected diffuse line, the surface power distribution pattern is shown in Figure 6(b). The power distribution pattern depends largely on the propagation path and multiple reflections across the room. For the case of LOS simulation, a 3.2 dB power variation was obtained with a maximum power of 80 μW received when the receiver was

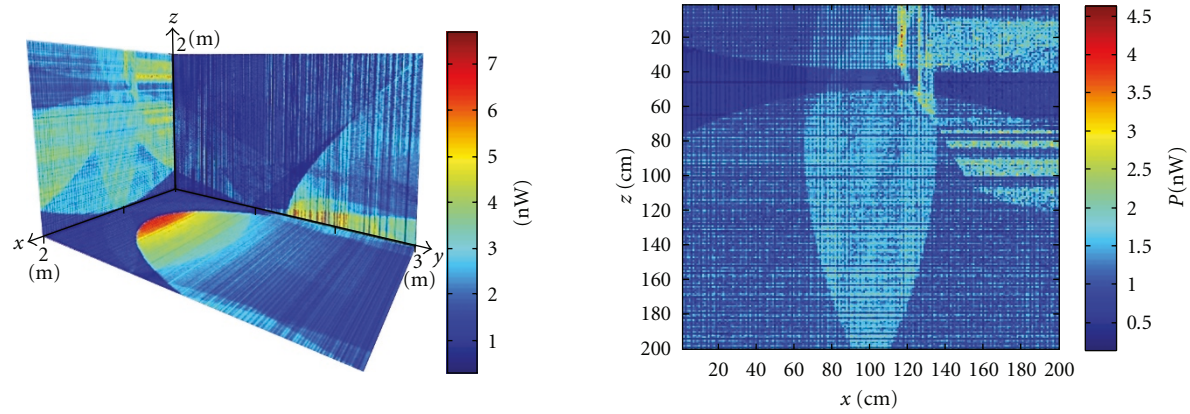

Figure 5: The surface power distributions with rays tracing up to 5 reflections for (a) three walls and (b) one wall.

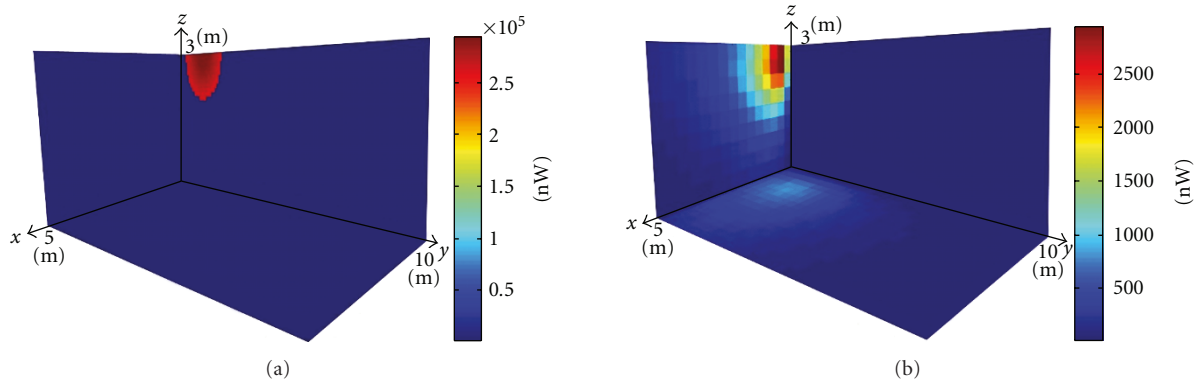

Figure 6: The surface power distributions of the walls for (a) LOS simulation and (b) nondirection diffuse simulation.

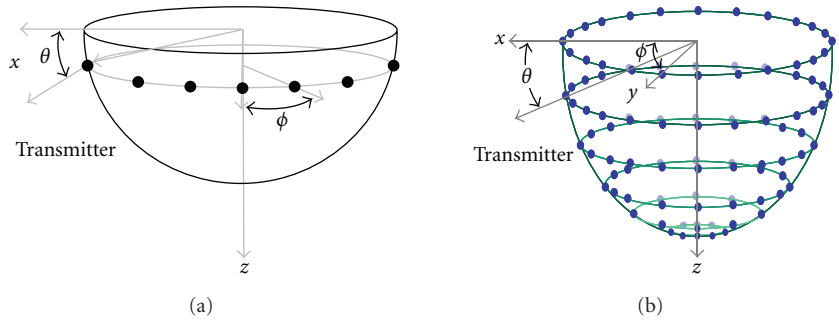

Figure 7: Multibeam transmitter structures for (a) 180-degrees ring shape and (b) hemisphere.

Table 1: Simulation parameters for a typical diffusive optical channel with one transmitter located at the ceiling.

Parameter	Value
Transmitter elevation angle and azimuth angle (θ, ϕ)	(30, 0) (degrees)
Transmitter position: (x, y, z)	(1, 1.5, 2) (m)
Room dimension: length, width, height	(i) $2.0 \times 3.0 \times 2.0$ (m) (ii) $10.0 \times 5.0 \times 2.0$ (m)
Reflection coefficients	Walls, ceiling, floor: 0.8, 0.8, 0.8
Number of reflections or bounces	5
Pixel size	0.01×0.01 (m)
Time interval Δt	2 ns

placed at the middle of the room. While for power coverage relying on the reflectivity of the ceiling and walls, a large path loss was observed due to the lack of a LOS optical path. A maximum received power of 2.5 μW was observed with a 2.5 dB variation in optical power across the room.

3.2. Design of Multibeam Transmitter. To achieve a near 180-degree omnidirectional transmission and reduce multipath distortion from numerous reflections, five configurations of multibeam transmitter design, as illustrated in Figure 7, were proposed. The parameters of these five configurations (labeled as A, B, C, D, and E) are shown in Table 2. The first multibeam transmitter or configuration A, illustrated as Figure 7(a), forming a shape of ring on a horizontal plane (xy plane), is constructed by 12 nonoverlapping transmitters such that each transmitter has the same elevation angles θ's but different azimuth angles ϕ's. The azimuth angles are arranged such that the angle separation between any two nearest neighborhood transmitters is 30 degrees. In xy plane, the proposed multibeam transmitter (configuration A) forms a circle that was connected by 12 individual transmitters. This configuration is essentially the basic structure of our proposed multibeam transmitter. The other configurations are constructed by either changing the azimuth angles of configuration A or assembling several of them into a certain shape. For example, configuration B and C have the same spatial distributions as configuration A except that they have different arrangement of azimuth angles. As shown in Table 2, the azimuth angles of the entire individual transmitter for configuration A, B, and C are 0°, 30°, and 60°, respectively. The configuration D consisting of 37 transmitters is constructed by four rings such that each ring is oriented with different elevation angle, ranging from 0° to 90° with an angle interval of 30 degrees. There are 12 transmitters for those three rings that have elevation angles of 0°, 30°, and 60°, respectively, and only one transmitter in the ring that has azimuth angle of 90°. The arrangement of azimuth angles for 12 transmitters is the same as of that in configuration A.

Configuration E is the most complicated design of multibeam transmitter among others. However, compared to other designs, this configuration can provide much higher power coverage and reduce multpath losses significantly. As shown in Figure 7(b), this configuration is constructed by seven rings with various transmitters that inherent from configuration A, forming a shape of hemisphere. There are in total 102 nonoverlapping transmitters distributed symmetrically among 7 different rings in this configuration. The elevation angle of the top ring is 0° and the difference of elevation angle between any two nearest neighborhood ring is 15 degrees. The number of transmitters in each ring is dependent on the elevation angle of the ring pointed, which are 24, 23, 20, 16, 12, 6, and 1 for elevations angles of 0°, 15°, 30°, 45°, 60°, 75°, and 90°, respectively. We have studied the performance for both LOS link and diffuse link with these five configurations. The LOS link simulation into one wall for configurations A, B, C, D, and E are shown in Figures 8(a)–8(d) and Figure 9(a), respectively. The diffuse link simulation with the first bounce of reflection into one wall are shown in Figures 8(e)–8(h), and those of the fifth bounce of reflection are depicted in Figures 8(i)–8(l) and Figure 9(b), respectively.

The impulse response of a typical receiver positioned in any location of the room was calculated and its performance across the room was evaluated. As shown in Figures 10 and 11, based on the parameters of a receiver in Table 2 we present the simulated impulse responses as a function of arrival time traced with number of bounces k = 0, 1, 2, 3, 4, and 5, for configurations D and E, respectively. These impulse responses are received optical intensity when the transmitted intensity from the source is a unit area Dirac delta function. The time origin is defined as the arrival of the LOS impulse. The numbers in parenthesis is the percentage of received power. It can be seen that configuration E has a higher peak performance than that of configuration D. However, their performance is several hundred times better than that of the traditional single transmitter presented in previous subsection. Total received power for both configurations is gradually decreased for each of the higher order impulse responses; however, for configuration D the contributions of low-order impulse responses dominate (more than 50% for $k < 2$) but for configuration E that of higher-order impulses responses still can add to a significant amount ($\sim$10% for $k = 5$) in the total power received.

Taking the Fourier transform of the impulse response provide us the frequency response and channel bandwidth for configuration D and E as shown in Figure 12. The 3 dB bandwidth for configuration D and E were about 38 MHz and 40 MHz, respectively, indicating that a symbol-spacing of as low as 25 ns may be achieved given the channel impulse response. The data rates we simulate are around 4 Mb/s for a single element transmitter. We expect that an optimized multibeam transmitter can reach data rates of about several 100 Mb/s in place of the LED by the high-efficiency laser diode.

The powers from high-order impulses responses play an important role in the link budget for they arrive much later than that of impulse responses from lower-order reflections. The simulation results for configurations A, B, C exhibited similar trends. However, their performance was about few times less than that of configurations C and D in terms of power coverage and speed. In summary, the simulation results show that higher-order reflections are still significant for both configurations and their power distributions have a wide angle range of coverage ($\sim$180 degrees) within a short duration time of 50 ns. Therefore, these proposed configurations, in particular for configuration E, can provide high speed and wide power coverage for indoor wireless infrared applications.

The receiver is scanned through the room allowing a bit error rate (BER) map to be determined. A crude estimation of BER can be performed by using a simple modulation and detection scheme, which is based on a baseband on-off keyed system as the one that illustrated by Barry et al. [9]. As the power radiation patterns of the room are obtained, the average SNR can be determined by averaging the transmitted optical intensity and received optical signal with an additive white Gaussian noise applied to the system. The average SNR

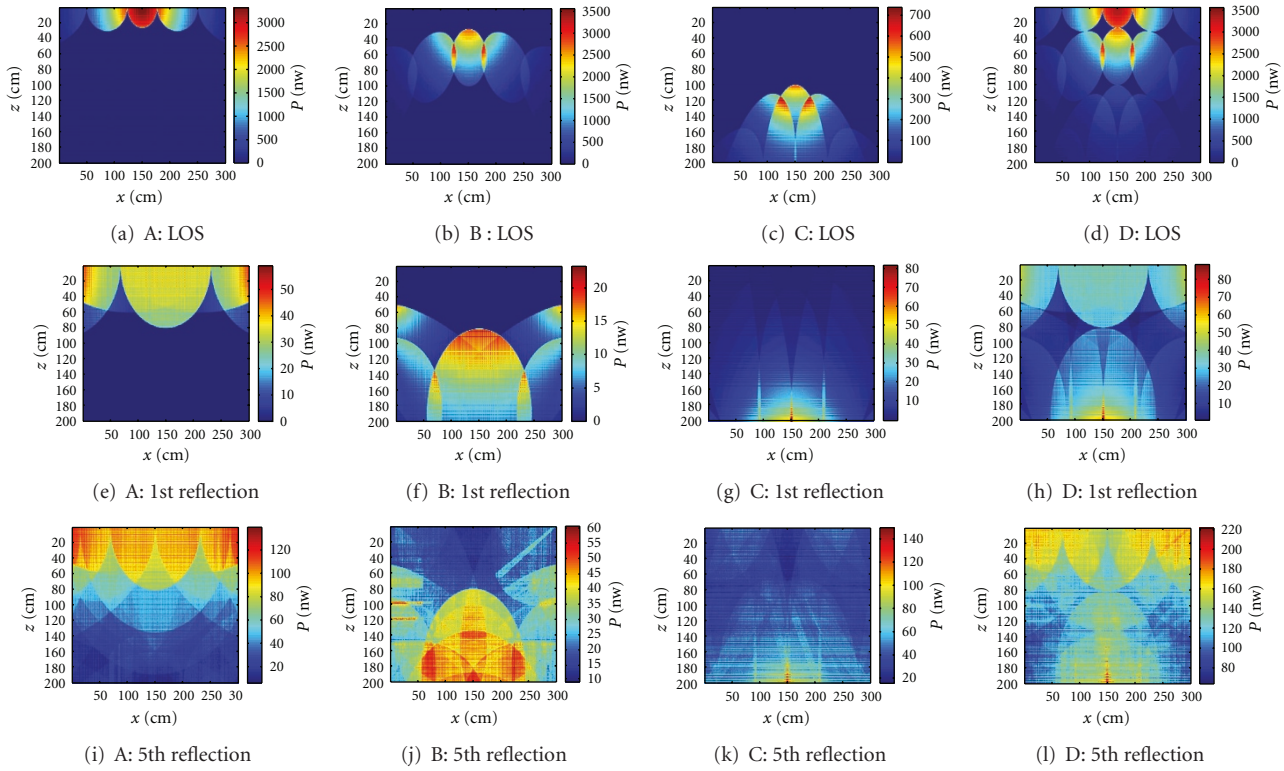

(a) A: LOS (b) B : LOS (c) C: LOS (d) D: LOS

(e) A: 1st reflection (f) B: 1st reflection (g) C: 1st reflection (h) D: 1st reflection

(i) A: 5th reflection (j) B: 5th reflection (k) C: 5th reflection (l) D: 5th reflection

Figure 8: Simulation results of surface power illumination pattern for configurations A, B, C, and D (from left to right in each row): (a)–(d) for LOS path, (e)–(h) for the first bounce of reflection on the wall, and (i)–(l) for the fifth bounce of reflection on the wall.

Table 2: Simulation parameters for five configurations of multibeam transmitters.

Parameter	A	B	C	D	E
Room:					
Length (x)	3 m	3 m	3 m	3 m	3 m
Width (y)	2 m	2 m	2 m	2 m	2 m
Height (z)	2 m	2 m	2 m	2 m	2m
Wall, ceiling reflectivity	0.8	0.8	0.8	0.8	—
Source:					
mode	1	1	1	1	1
x	1.5 m	1.5 m	1.5 m	1.5 m	1.5 m
y	1 m	1 m	1 m	1 m	1 m
z	2 m	2 m	2 m	2 m	2 m
Power	1 W	1 W	1 W	1 W	1 W
Elevation	0°	30°	60°	0°–90°	0°–90°
Azimuth	0°–360°	0°–360°	0°–360°	0°–360°	—
Number of transmitters	12	12	12	37	102
Receiver:					
Area	1 cm^2	1 cm^2	1 cm^2	1 cm^2	1 cm^2
FOV	90°	90°	90°	90°	90°
(x, y, z) (m)	(1.5,1,0)	(1.5,1,0)	(1.5,1,0)	(1.5,1,0)	(1.5,1,0)
Resolution:					
Pixel elements	320000	320000	320000	320000	320000
Δt	2 ns	2 ns	2 ns	2 ns	2 ns
Bounces	5	5	5	5	5
Ray division (radian)	1/2000	1/2000	1/2000	1/2000	1/100000
Ray numbers	5955959	12620557	16596235	36830445	—

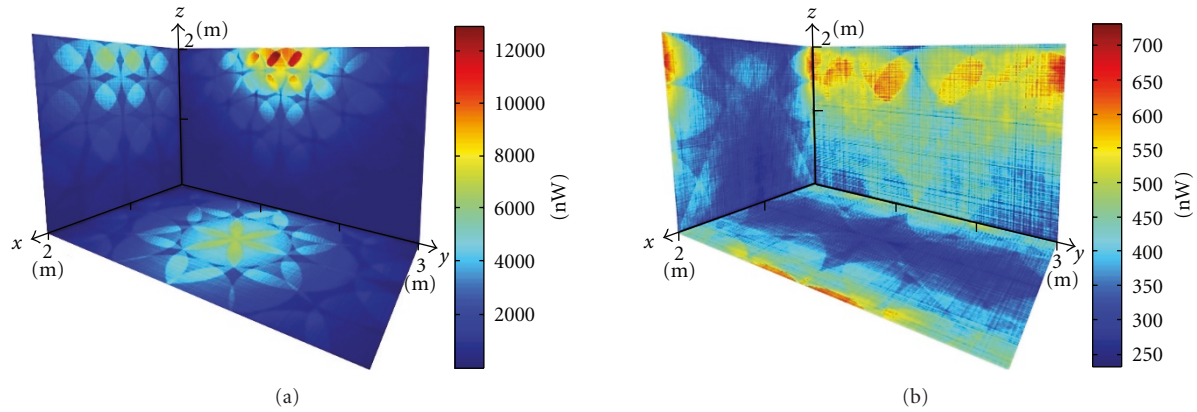

Figure 9: Simulation results of surface power-delay illumination pattern for configuration E: (a) for LOS path and (b) for the fifth bounce of reflection on the wall.

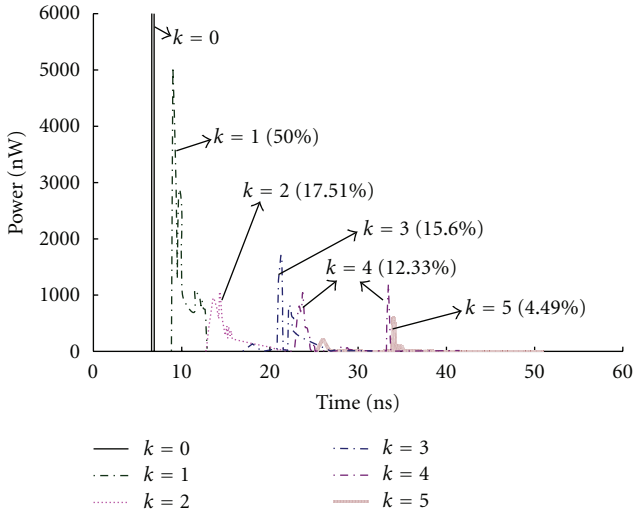

Figure 10: Impulse responses of configuration D for light undergoing up to five reflections.

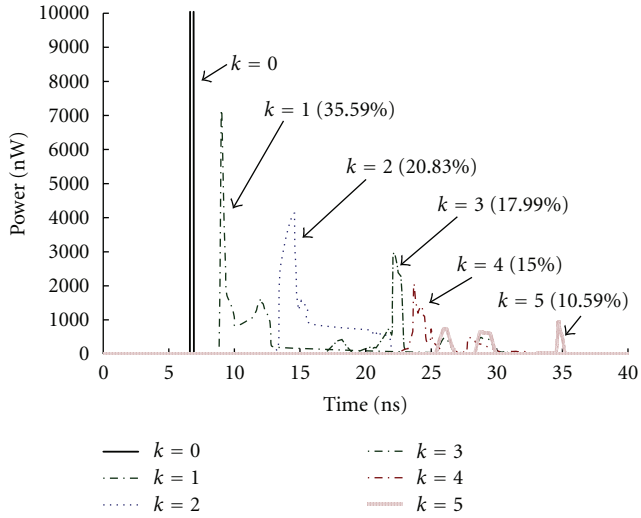

Figure 11: Impulse responses of configuration E for light undergoing up to five reflections.

will then be used to calculate the BER using the Gaussian Q function in (16). BER less than 10^{-7} (average SNR = 14.3 dB) can be easily achieved using the proposed configuration E. Several factors such as the dimensions of the room, reflection coefficients, FOV of receiver elements can be easily adjusted and their influences to the performance of high bit rate can be studied. For example, a five more times reduction of the number of LEDs or lasers in the proposed transmitter system, BER less than 10^{-5} (average SNR = 12.6 dB) is achieved. To significantly enhance its BER performance, the proposed system can be used in joint with a high-resolution imaging angle diversity receiver.

3.3. Optimization of Multibeam Transmitter Design. Based on the simulation results the multibeam transmitter (such as configuration E) proposed here is capable of offering extremely high speed and wide coverage of power distributions for indoor wireless communications. However the power uniformity of the transmitter has yet to be optimized. For high performance wireless diffuse links with uniform power illumination distributions, as illustrated in Figure 1, the best design of such a transmitter is enabled to provide a constant and steady power distribution across the coverage area (or working area) and its LOS signal (red light lines in Figure 1) significantly overpasses the multiple reflected impulse responses or non-LOS signals (red dot light lines in Figure 1). In this wireless system the users moving around the room can easily and quickly receive the signal from the transmitter without any significant time delay and power variation.

Assuming that the detected signal power is constant and uniform (almost no power variation can be measured) in any location of a rectangle room, using the multipath diffusive propagation model we compute the corresponding optimized radiation intensity pattern by a transmitter placed at the center of the ceiling. Figure 13 shows the result of

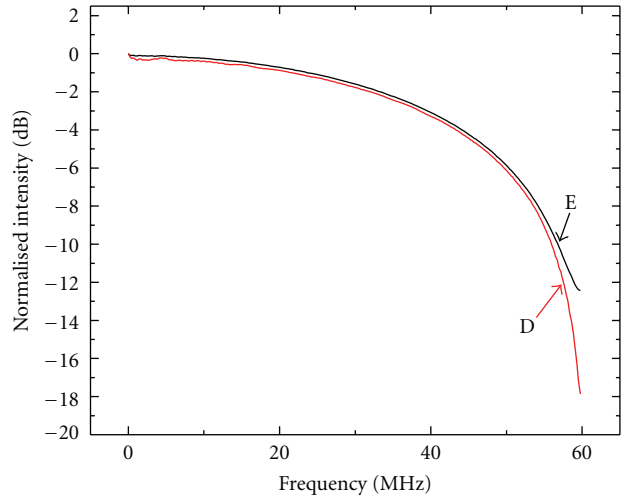

Figure 12: Frequency responses for configuration D and E as light undergoing up to five reflections.

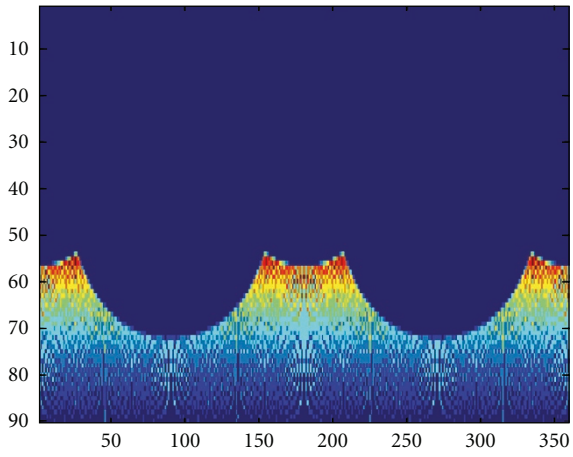

Figure 13: Optimized radiation intensity pattern of the transmitter (see text).

the radiation intensity pattern as a function of elevation angle (vertical axis) and azimuth angle (horizontal axis). Any design of the transmitter structure that fulfills the predicted power distributions as shown in Figure 13 should be able to provide a uniform and full coverage of power distributions and this can be achieved by modifying some key parameters of the multibeam transmitter, such as the number of transmitters, elevation and azimuth angle, geometry, position, and power profile. There have been many attempts in designing the transmitter to achieve uniform radiation pattern. To our knowledge, this is the first that such a uniform radiation pattern has been designed. Future work to develop this optimized transmitter design and maximize its channel performance is underway.

4. Conclusions

We have presented a multipath diffusive propagation model for evaluating the impulse response of an arbitrary room with Lambertian sources and reflectors. The method can account for any number of reflecting paths. Using this model we proposed several multibeam transmitter systems for future highspeed indoor wireless diffuse links that can provide the full coverage of field of view as well as the power receiving performance.

The simulation method presented here allows a wide range of transmitter configurations to be evaluated in a timely manner, which provides a useful tool to design complex transceiver structures for high bit rate system and optimize the power to be collected or emitted. Future work will focus on both measurement and simulation of this technique especially for developing the optimized transmitter design proposed in this paper.

Acknowledgment

This work was partially supported by the National Science Council (NSC) of Taiwan.

References

[1] F. R. Gfeller and U. Bapst, "Wireless in-house data communication via diffuse infrared radiation," *Proceedings of the IEEE*, vol. 67, no. 11, pp. 1474–1486, 1979.

[2] G. Yun and M. Kavehrad, "Spot diffusing and Fly-Eye receivers for indoor infrared wireless communications," in *Proceedings of the IEEE International Conference on Selected Topics in Wireless Communication*, pp. 286–292, Vancouver, B.C., Canada, 1992.

[3] J. R. Barry, *Wireless Infrared Communications*, Klumer Academic publishers, Boston, Mass, USA, 1994.

[4] A. M. Street, P. N. Stavrinou, D. C. O'Brien, and D. J. Edwards, "Indoor optical wireless systems—a review," *Optical and Quantum Electronics*, vol. 29, no. 3, pp. 349–378, 1997.

[5] D. J. T. Heatley, D. R. Wisely, I. Neild, and P. Cochrane, "Optical wireless: the story so far," *IEEE Communications Magazine*, vol. 36, no. 12, pp. 72–82, 1998.

[6] R. M. Gagliardi and S. Karp, *Optical Communication*, John Wiley & Sons, New York, NY, USA, 2nd edition, 1995.

[7] J. M. Kahn and J. R. Barry, "Wireless infrared communications," *Proceedings of the IEEE*, vol. 85, pp. 265–298, 1997.

[8] J. M. H. Elmirghani, H. H. Chan, and R. A. Cryan, "Sensitivity evaluation of optical wireless PPM systems utilising PIN-BJT receivers," vol. 143, no. 6, pp. 355–359.

[9] J. R. Barry, J. M. Kahn, W. J. Krause, E. A. Lee, and D. G. Messerchmitt, "Simulation of multipath impulse response for indoor wireless optical channels," *IEEE Journal on Selected Areas in Communications*, vol. 11, no. 3, pp. 367–379, 1993.

[10] S. Arnon, D. M. Britz, A. C. Boucouvalas, and M. Kavehrad, "Optical wireless communications: introduction to the feature issue," *Journal of Optical Networking*, vol. 5, no. 2, pp. 79–81, 2006.

[11] Z. Ghassemlooy and A. C. Boucouvalas, "Guest editorial: indoor optical wireless communication systems and networks," *International Journal of Communication Systems*, vol. 18, no. 3, pp. 191–193, 2005.

[12] A. P. Tang, J. M. Kahn, and K. Ho, "Wireless infrared communication links using multi-beam transmitters and imaging receivers," in *Proceedings of the IEEE International Conference on Communications (ICC '96)*, pp. 180–186, Dallas, Tex, USA, June 1996.

[13] P. Djahani and J. M. Kahn, "Analysis of infrared wireless links employing multibeam transmitters and imaging diversity receivers," *IEEE Transactions on Communications*, vol. 48, no. 12, pp. 2077–2088, 2000.

[14] J. M. Kahn, R. You, P. Djahani, A. G. Weisbin, K. T. Beh, and A. Tang, "Imaging diversity receivers for high-speed infrared wireless communication," *IEEE Communications Magazine*, vol. 36, no. 12, pp. 88–94, 1998.

[15] T. J. Svetla and M. Kavehrad, "Multispot diffusing configuration for wireless infrared access," *IEEE Transactions on Communications*, vol. 48, no. 6, pp. 970–978, 2000.

[16] J. B. Carruthers and J. M. Kahn, "Angle diversity for nondirected wireless infrared communication," *IEEE Transactions on Communications*, vol. 48, no. 6, pp. 960–969, 2000.

[17] J. M. Kahn, W. J. Krause, and J. B. Carruthers, "Experimental characterization of non-directed indoor infrared channels," *IEEE Transactions on Communications*, vol. 43, no. 2, pp. 1613–1623, 1995.

[18] M. R. Pakravan, E. Simova, and M. Kavehrad, "Holographic diffusers for indoor infrared communication system," in *Proceedings of the 1996 IEEE Communications Theory Mini-Conference*, vol. 3, pp. 1608–1612, November 1996.

[19] G. N. Bakalidis, E. G. Lavas, and P. Tsalides, "Optical power distribution in wireless infrared LANs," *IEE Proceedings, Optoelectronics*, vol. 143, no. 2, pp. 93–97.

[20] J. B. Carruthers and J. M. Kahn, "Angle diversity for nondirected wireless infrared communication," in *Proceedings of the 1998 IEEE International Conference on Communications (ICC '98)*, vol. 3, pp. 1665–1670, June 1998.

[21] J. M. Kahn, R. You, P. Djahani, A. G. Weisbin, B. K. Teik, and A. Tang, "Imaging diversity receivers for high-speed infrared wireless communication," *IEEE Communications Magazine*, vol. 36, no. 12, pp. 88–94, 1998.

[22] P. Djahani and J. M. Kahn, "Analysis of infrared wireless links employing multi-beam transmitters and imaging diversity receivers," in *Proceedings of the IEEE Global Telecommunications Conference (GLOBECOM '99)*, vol. 1, pp. 497–504, 1999.

[23] S. Jivkova and M. Kavehrad, "Indoor wireless infrared local access, multi-spot diffusing with computer generated holographic beam-splitters," in *Proceedings of the IEEE International Conference Communications (ICC 9'9)*, pp. 604–608.

[24] S. Jivkova and M. Kavehrad, "Receiver designs and channel characterization for multi-spot high-bit-rate wireless infrared communications," *IEEE Transactions on Communications*, vol. 49, no. 12, pp. 2145–2153, 2001.

[25] S. Jivkova, B. A. Hristov, and M. Kavehrad, "Power-efficient multispot-diffuse multiple-input-multiple-output approach to broad-band optical wireless communications," *IEEE Transactions on Vehicular Technology*, vol. 53, no. 3, pp. 882–889, 2004.

[26] H. Yang and C. Lu, "Infrared wireless LAN using multiple optical sources," *IEE Proceedings: Optoelectronics*, vol. 147, no. 4, pp. 301–307, 2000.

[27] A. G. Al-Ghamdi and J. M. H. Elmirghani, "Line strip spot-diffusing transmitter configuration for optical wireless systems influenced by background noise and multipath dispersion," *IEEE Transactions on Communications*, vol. 52, no. 1, pp. 37–45, 2004.

[28] A. G. Al-Ghamdi and J. M. H. Elmirghani, "Spot diffusing technique and angle diversity performance for high speed indoor diffuse infra-red wireless transmission," *IEE Proceedings: Optoelectronics*, vol. 151, no. 1, pp. 46–52, 2004.

[29] A. G. Al-Ghamdi and J. M. H. Elmirghani, "Performance analysis of mobile optical wireless systems employing a novel beam clustering method and diversity detection," vol. 151, pp. 223–231.

[30] A. G. Al-Ghamdi and J. M. H. Elmirghani, "Analysis of diffuse optical wireless channels employing spot-diffusing techniques, diversity receivers, and combining schemes," *IEEE Transactions on Communications*, vol. 52, no. 10, pp. 1622–1631, 2004.

[31] A. Sivabalan and J. John, "Improved power distribution in diffuse indoor optical wireless systems employing multiple transmitter configurations," *Optical and Quantum Electronics*, vol. 38, no. 8, pp. 711–725, 2006.

[32] A. Sivabalan and J. John, "Effect of transmitter positions on received power and bandwidth in diffuse indoor optical wireless systems," *Optical and Quantum Electronics*, vol. 39, no. 1, pp. 1–14, 2007.

[33] J. G. Fernandes, P. A. Watson, and J. C. Neves, "Wireless LANs: physical properties of infra-red systems vs. MMW systems," *IEEE Communications Magazine*, pp. 68–73, 1994.

[34] R. Pérez-Jiménez, J. Berges, and M. J. Betancor, "Statistical model for the impulse response on infrared indoor diffuse channels," *Electronics Letters*, vol. 33, no. 15, pp. 1298–1300, 1997.

[35] F. J. López-Hernández and M. J. Betancor, "DUSTIN: algorithm for calculation of impulse response on IR wireless indoor channels," *Electronics Letters*, vol. 33, no. 21, pp. 1804–1806, 1997.

[36] F. J. López-Hernández, R. Pérez-Jiménez, and A. Santamaría, "Monte Carlo calculation of impulse response on diffuse IR wireless indoor channels," *Electronics Letters*, vol. 34, no. 12, pp. 1260–1262, 1998.

[37] F. J. López-Hernández, R. Pérez-Jiménez, and A. Santamaría, "Modified Monte Carlo scheme for high-efficiency simulation of the impulse response on diffuse IR wireless indoor channels," *Electronics Letters*, vol. 34, no. 19, pp. 1819–1820, 1998.

[38] J. B. Carruthers and J. M. Kahn, "Modeling of nondirected wireless infrared channels," *IEEE Transactions on Communications*, vol. 45, no. 10, pp. 1260–1268, 1997.

[39] J. B. Carruthers and P. Kannan, "Iterative site-based modeling for wireless infrared channels," *IEEE Transactions on Antennas and Propagation*, vol. 50, no. 5, pp. 759–765, 2002.

[40] J.-L. Tang, P. C. Jui, and S. C. Wang, "Simulation and design of omni-directional high-speed multi-beam transmitter system," in *Optical Transmission, Switching, and Subsystems IV*, C. Pak, S. Xie, C. R. Menyuk, and K. Kitayama, Eds., vol. 6353 of *Proceedings of SPIE*, 2006.

[41] A. S. Glassner, Ed., *An Introduction to Ray Tracing*, Academic Press, San Diego, Calif, USA, 1989.

[42] D. Hash, J. Hillery, and J. White, "IR roomnet: model and measurement," in *Proceedings of the International IBM Common Conference*, June 1986.

[43] W. J. Krause, *Experimental characterization of non-directed indoor infrared channels*, M.S. thesis, Univesity of California, Berkely, Calif, USA, 1993.